Molecular Crystals and Liquid Crystals

Publication details, including instructions for authors and subscription information:
http://www.tandfonline.com/loi/gmcl20

Optical Structures and their Control in a Liquid-Crystal-Light-Valve Experiment

U. Bortolozzo [a b], S. Residori [a] & P. L. Ramazza [b]

[a] Institut Non Linéaire de Nice, Valbonne, France

[b] Istituto dei Sistemi Complessi, CNR, Florence, Italy

Version of record first published: 31 Aug 2006

To cite this article: U. Bortolozzo, S. Residori & P. L. Ramazza (2006): Optical Structures and their Control in a Liquid-Crystal-Light-Valve Experiment, Molecular Crystals and Liquid Crystals, 450:1, 141/[341]-162/[362]

To link to this article: http://dx.doi.org/10.1080/15421400600587936

Mol. Cryst. Liq. Cryst., Vol. 450, pp. 141/[341]–162/[362], 2006

ISSN: 1542-1406 print/1563-5287 online
DOI: 10.1080/15421400600587936

Optical Structures and their Control in a Liquid-Crystal-Light-Valve Experiment

U. Bortolozzo
Institut Non Linéaire de Nice, Valbonne, France and
Istituto dei Sistemi Complessi, CNR, Florence, Italy

S. Residori
Institut Non Linéaire de Nice, Valbonne, France

P. L. Ramazza
Istituto dei Sistemi Complessi, CNR, Florence, Italy

We review the conditions for the control of optical structures in a nonlinear optical experiment, which is a Liquid-Crystal-Light-Valve with optical feedback. The optical structures we deal with may be either localized states or spatially extended patterns. Indeed, the localized structures here described represent the localized solutions of a pattern-forming system. We will show that there exists different regions of existence of such localized states, and that different types of localized structures can be selected depending on the choice of the control parameters. Localized states, stable for some range of parameters, are in general characterized by complex spatio-temporal dynamics. In the same way, spatially extended patterns show space-time chaotic behaviors. We show that pattern targeting and control may be achieved by adding an extra control loop to the experiment. Different target patterns can be stabilized in real time and synchronization between space-time chaotic signals is demonstrated.

Keywords: liquid crystal light valves; localized structures; pattern control and targeting; space-time chaos synchronization

INTRODUCTION

Nonequilibrium processes lead in nature to the formation of spatially periodic and extended structures, so-called patterns [1]. The birth of a pattern from a homogeneous state takes place through the

Address correspondence to U. Bortolozzo, Institut Non Linéaire de Nice, UMR 6618 CNRS-UNSA, 1361 Route des Lucioles, F-06560 Valbonne, France. E-mail: umberto.bortolozzo@inln.cnrs.fr

spontaneous breaking of one or more of the symmetries characterizing the system [2]. In some cases, the pattern is localized in a particular region of the available space, so that we deal with localized instead of extended structures. From a theoretical point of view, localized structures in out of equilibrium systems can be seen as a sort of dissipative solitons [3]. Experimentally, during the last years localized patterns or isolated states have been observed in many different fields, such as magnetic materials [4], liquid crystals [5], gas discharge experiments [6], chemical reactions [7], granular media [9], surface waves [8], thermal convection [10,11].

In nonlinear optics dissipative solitons have first been predicted to appear in bistable ring cavities [12]. Then, localized states have been largely studied not only for their fundamental properties but also in view of their potential applications in photonics [13–16]. Sometimes named as cavity solitons, optical localized structures have been observed in photorefractive materials [17], in lasers with saturable absorber [18], in Liquid-Crystal-Light-Valves (LCLVs) with optical feedback [19,20], in Na vapors [21] and in semiconductor microcavities [22]. These localized states can be considered to belong to the same general class of localized structures, that is, they are patterns that extend only over a small portion of a spatially extended system. The mechanisms of localization of spatial structures rely on two mains ingredients: the bistability, either between two homogeneous states or between a homogeneous state and a spatially modulated one, and the existence of an intrinsic spatial length, that is necessary to stabilize a localized state and which determines its typical size [23].

In order to take advantage of localized structures for photonics applications, it appears essential to understand the conditions for their stable localization as well as their intrinsic dynamical behaviors [24]. Here, we review the conditions for the appearance of stable localized states in a nonlinear optical system, which is a LCLV with optical feedback. In this system the bistability between homogenous states results from the subcritical character of the Fréedericksz transition, when the local electric field, which applies to the liquid crystals, depends on the liquid crystal reorientation angle [25]. In the optical feedback loop, the bistability is present together a pattern forming diffraction length. This ensures the presence of the two necessary ingredients, bistability and a critical length scale, for the appearance of localized structures. We will also review the different types of localized states that may be selected depending on the choice of the different regions of parameters. In particular, we will show that it exists a bistability between two different types of localized structures, having, respectively, a round and a triangular shape [26].

Then, we present the control and targeting [27] of patterns, that are stabilized over spatio-temporal chaos by means of a real space/real-time control technique. We also show how this control technique allows to synchronize space-time chaotic signals [28].

The article is divided as follows. In section 2 we present the experiment, whereas in section 3 we show the appearance of localized structures, their dynamical behaviors and their different type. In section 4, we present a method to control the pattern formation and to induce the synchronization of spatio-temporal chaotic signals. Section 5 are the conclusions.

DESCRIPTION OF THE EXPERIMENT

The experiment, shown in Figure 1, consists of a LCLV with optical feedback, as it was originally designed by the Akhmanov group [29].

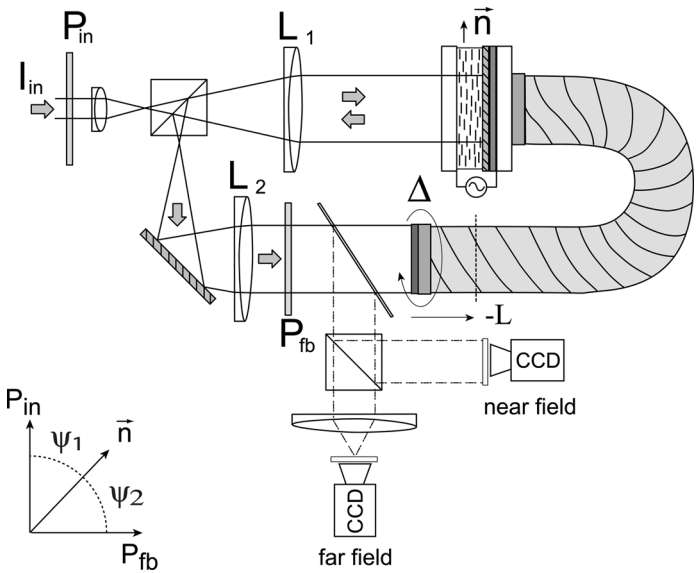

FIGURE 1 Experimental setup: the LCLV is illuminated by a plane wave; the wave, reflected by the dielectric mirror inside the LCLV, is sent back to the photoconductor through the optical fiber bundle. Δ is the angle of rotation of the fiber with respect to the front side of the LCLV. $\vec{n}$ is the liquid crystal nematic director; P_{in} and P_{fb} are the input and feedback polarizers; L_1 and L_2 are two confocal 25 cm focal length lenses. $-L$ is the free propagation length, negative with respect to the plane on which a 1:1 image of the front side of the LCLV is formed.

The LCLV is composed of a nematic liquid crystal film sandwiched in between a glass window and a photoconductive plate over which a dielectric mirror is deposed. Coating of the bounding surfaces induces a planar anchoring of the liquid crystal film (nematic director $\vec{n}$ parallel to the walls). Transparent electrodes covering the two confining plates permit the application of an electric field across the liquid crystal layer. The photoconductor behaves like a variable resistance, which decreases for increasing illumination. The feedback is obtained in the following way: the light which has passed through the liquid-crystal layer, and has been reflected by the dielectric mirror inside the LCLV, is sent back onto the photoconductor of the LCLV. This way, the light beam experiences a phase shift which depends on the liquid crystal reorientation and, on its turn, modulates the effective voltage that locally is applied to the liquid crystals. Thus, a feedback is established between the liquid crystal reorientation and the local electric field.

Transverse patterns in the optical field are recorded by two CCD cameras, one collecting the near-field light distribution and one recording the light intensity in the focal plane of a lens, that is, the far-field patterns. The laser beam is expanded up to a diameter of 3 cm, whereas the transverse size of the LCLV is of 2.5 cm. A circular diaphragm, whose diameter is typically set to 1 cm, is inserted in front of the LCLV, so that only a central region is active, which is uniformely illuminated.

Patterns arises because of feedback, which converts the phase modulation generated within the LCLV by the liquid crystal reorientation into intensity modulation. On its turns, this drives the effective voltage applied to the liquid crystal film by changing the impedance of the photoconductor. Typical time constants of the LCLV are of the order of tens of milliseconds, whereas the round-trip time of the light is of the order of few nanoseconds. Thus, the feedback can be considered as instantaneous and the light field always at equilibrium with the liquid crystal reorientation.

The feedback loop is closed by an optical fiber bundle, with one end mounted on a precision rotation stage allowing to fix the feedback rotation rotation angle Δ with a precision of $\pm 0.01^{\circ}$. In the set of experiments presented here Δ is fixed to 0°, so that there is no image rotation in the feedback loop. Two kinds of optical feedback may be set in the experiment. Indeed, phase to amplitude conversion can be achieved either by diffraction or by polarization interference [30]. Two polarizers are inserted in the optical loop: P_{in} selects the polarization of the input light whereas P_{fb} controls the polarization of the feedback light; ψ_1 and ψ_2 are the angles formed by the input and feedback

light polarization with the liquid crystal director $\vec{n}$, respectively. Polarization interference arises whenever $\psi_1, \psi_2 \neq 0°$. In particular, for $\psi_1 = -\psi_2 = 45°$ the ordinary and extraordinary components contributes in the same way to the feedback, so that the contrast of polarization interference is maximized. If $L=0$ (purely interferential case) patterns arise only in the presence of a nonlocal feedback, due either to rotation or lateral displacement of the optical fibre bundle, otherwise the system displays bistability between homogeneous states and fronts connecting the two metastable states [25].

The purely diffractive case corresponds to setting $\psi_1=\psi_2=0°$ with $L\neq 0$. In the presented set of experiments, the optical free propagation length is varied from $L=-30$ to $L=-100$ mm. Since the response of the LCLV can be assimilated to that of a Kerr medium, in the purely diffractive configuration the system is analogous to a Kerr-like nonlinear medium with optical feedback [31]. At the linear stage for the pattern formation, the theoretical model for such a system predicts successive branches of instability for pattern formation. A negative propagation distance, as we have chosen in our experiments, selects the first unstable branch of the marginal stability curve, as for a focusing Kerr-like nonlinearity [30].

In general, polarization interference and diffraction may be simultaneously present, contributing with different weights to the optical feedback. In such a case, by increasing the voltage applied to the LCLV, V_0, or the input light intensity, I_{in}, we observe successive branches of bistability between a homogenous state and a pattern state. Typical *r.m.s.* values for V_0 are in between 5 and 18 V and typical frequencies are in the range of 3 to 10 KHz. The total input intensity is typically in between $I_{in}=0.30\,\mathrm{mW/cm^2}$ and $I_{in}=1.00\,\mathrm{mW/cm^2}$.

LOCALIZED STRUCTURES

In the simultaneous presence of diffraction ($L\neq 0$) and polarization interference ($\psi_1 = -\psi_2 = 45°$), the system displays successive branches of bistability between an homogeneous state and a pattern state. A typical situation of this kind is sketched in Figure 2 where $\varphi_0=\beta\cos^2\theta$ is the nonlinear phase shift of the light that has passed through the LCLV, with θ the liquid crystal reorientation angle and $\beta=k\Delta n d$, where $k=2\pi/\lambda$ is the optical wave number, $\lambda=632$ nm is the laser wavelength, $\Delta n \simeq 0.2$ the liquid crystal birefringence and $d=15\,\mu$m the liquid crystal thickness. By increasing the input intensity I_{in}, the lower uniform branch is stable for a large portion, while the upper one is unstable. At a critical value for I_{in}, the lower branch becomes modulationally instable and gives rise to stable hexagons.

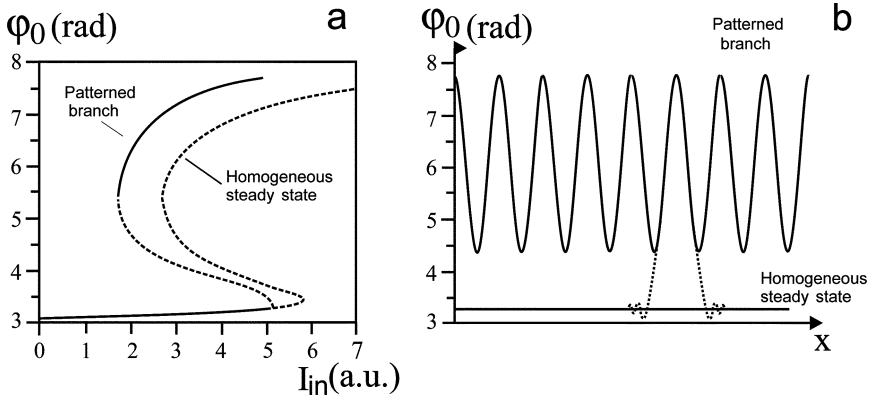

FIGURE 2 a) The homogeneous steady state characteristics of the LCLV system and its bifurcation to a patterned branch. Continuous linse: stable states. Dashed lines: unstable states. b) Formation of a localized structure, arising from the connection of a single pattern cell to the uniform background.

As depicted in Figure 2a, the bifurcation is subcritical. In the range of input intensities at which the hexagons coexist with the stable homogeneous state, localized structures can appear. A solution of this kind is shown in Figure 2b, where it is represented as a single cell of the hexagonal lattice connected to the low intensity homogeneous steady state. Analytical and numerical investigations have shown that this localized state is stable, because of the pinning effect which prevents the growth of one of the two solutions at the expenses of the other [34].

Here we review the typical localized structures that are observed in general when the system is close to a point of bistability. In the space of parameters, the points of bistability are identified as the locations where the surface of stationary states becomes s-shaped. Such a surface is represented in Figure 3, where the homogeneous equilibrium solutions for the liquid crystal reorientation angle θ_0 are plotted against the two control parameters of the experiments, that are the voltage applied to the LCLV, V_0, and the input light intensity, I_{in}. Because of the optical feedback, the voltage V that locally applies to the liquid crystal layer is $V = \Gamma V_0 + \alpha I_{fb}$, where Γ is the impedance of the LCLV dielectric layers, α is a phenomenological parameter resuming, in the linear approximation, the response of the LCLV and I_{fb} is the feedback light intensity:

$$I_{fb} = \frac{I_{in}}{2} |(1 + e^{-i\beta \cos^2 \theta})|^2 = I_{in}[1 + \cos(\beta \cos^2 \theta)].$$

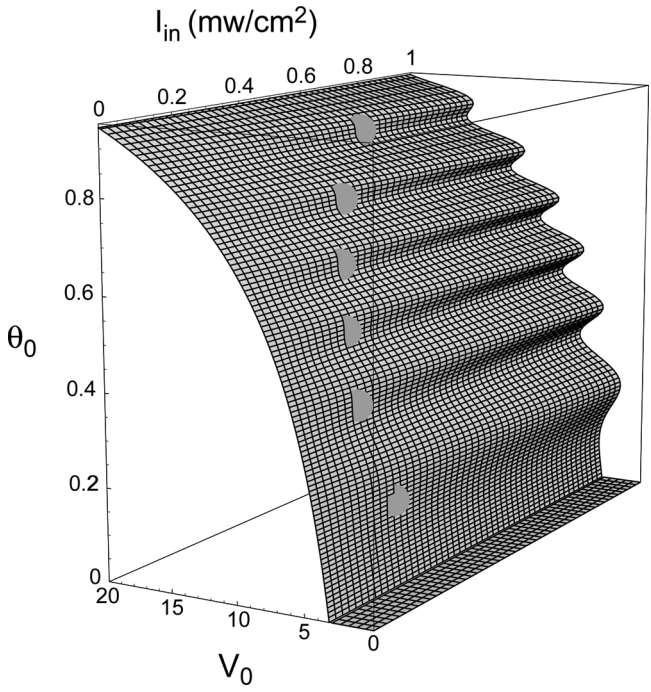

FIGURE 3 The multi-valued function $\theta_0(V_0, I_{in})$. Shaded areas show the locations where the system becomes bistable.

It can be shown that $\theta_0 = 0$ when $V \leq V_{FT}$ and $\theta_0 = \pi/2\left(1 - \sqrt{V_{FT}/V}\right)$ when $V > V_{FT}, V_{FT}$ being the Fréedericksz transition voltage [24].

Round Localized States and their Dynamics

The control parameters of the experiments are the applied voltage, V_0, and the input light intensity, I_{in}. Different sets of experiments may be performed either by fixing V_0 and varying I_{in} or by fixing I_{in} and changing V_0. This corresponds to different sections of the above surface. Localized structures appear close to each point of bistability and their size is approximately $\Lambda = 305\,\mu\text{m}$ for $L = -10\,\text{cm}$.

The distance between the spots is in average much larger than their individual size, which indicates that we deal with a collection of localized structures instead of a densely covered and extended pattern. However, when brought one close to the other, localized structures interact and form bound states, with two or more individual structures

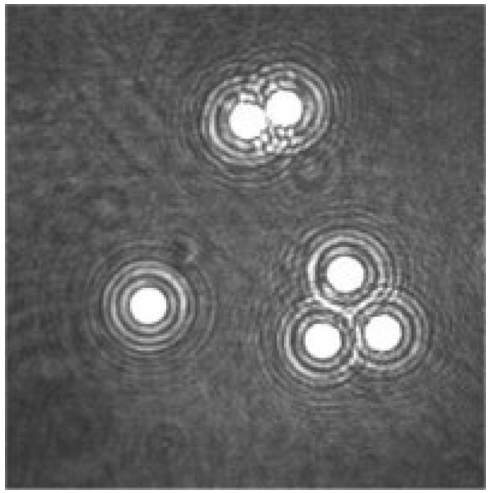

FIGURE 4 Examples of a single localized structure and of bound states.

coupled together [32]. Examples of localized structures and of their bound states are shown in Figure 4. The occurrence of this kind of localized structures has recently attracted a lot of interest, also in view of their application as pixels in devices for information storage and processing [33].

Localized structures are stable for some range of parameters, but a slight change in the input intensity I_{in} or V_0, can lead to complex dynamical behaviors, with the position of each localized structure oscillating periodically or chaotically during the time. In order to single out the localized structure dynamics without the influence of spatial inhomogeneities present in the LCLV, we have carried out one-dimensional experiments by inserting a rectangular mask in the optical feedback loop. The width D of the aperture is 0.50 mm whereas its length l is 20 mm. The transverse aspect ratio $D/\Lambda \simeq 1$ is small enough for the system to be be considered as one-dimensional whereas the longitudinal aspect ratio $l/\Lambda \simeq 60$ is large enough for the system to be considered as a spatially extended one.

In Figure 5 are shown the instantaneous snapshots of three adjacent localized structures, with two of them bouncing periodically in time one over the other. The corresponding spatial profiles are plotted below. Further increase of I_{in} or V_0 leads to aperiodic sequences of bouncing. For even further increase of I_{in} localized states eventually loose their stability.

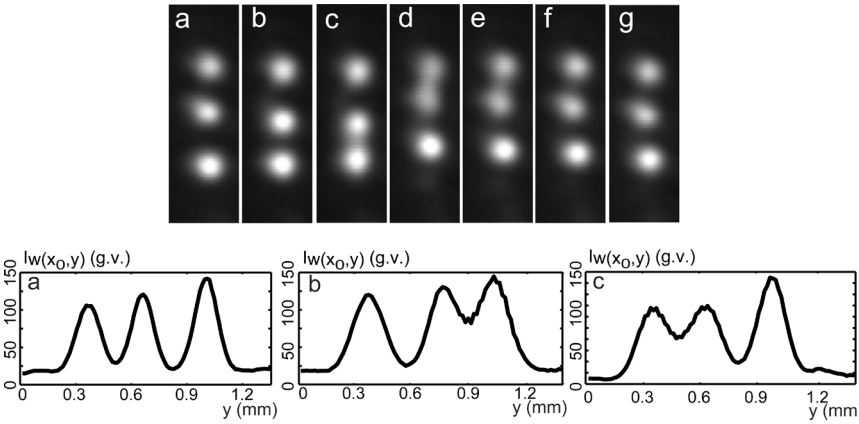

FIGURE 5 Instantaneous snapshots showing three bouncing localized structures. Times: a) 0.0, b) 1.0, c) 1.3, d) 1.7, e) 2.1, f) 2.4, and g) 2.8 s; $I_{in} = 0.90\,\mathrm{mW/cm^2}$ and $V_0 = 12.3\,\mathrm{V}$ (frequency 5 KHz). Bottom row: spatial profiles corresponding to times: a) 0.0, b) 1.3, and c) 1.7 s; g.v. are gary values on the CCD.

Bistability between Two Different Types of Localized States

We have recently shown that it exists a region of parameters where the LCLV experiment displays bistability between different types of localized structures [26]. The two kinds of localized states have different shape and different peak intensity. If used as pixels for information storage, the two amplitude levels of localized states give the possibility to define three-state variables, instead of the common two-state variables ("bits") that a single localized structure can encode. Consequently, use of the two types of structures would lead to an increase of $\log_2 3 \simeq 1.585$ for the information storable in a given area of the LCLV.

Bistability between localized structures is observed in the presence of two modulational instabilities having different critical wavenumbers. To realize this situation, we have set the system parameters at $L = 30\,\mathrm{mm}$, $V_0 = 5.8\,\mathrm{V}$ (frequency 8 KHz). The most evident feature of the new localized structure is its triangular symmetry, observed both in the central peak and in the tails. Hence, we have named this structure as *triangular localized structure*, in comparison with the usual *round localized structures* characterized by a circular symmetry. A triangular and a round localized structure is shown in Figure 6, where it can be noted that the state has a peak intensity much larger than the round one. Moreover, the size of the central peak is substantially

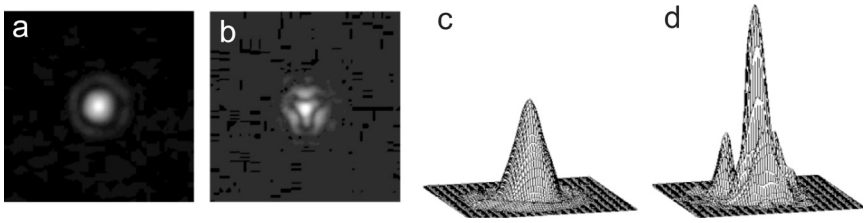

FIGURE 6 a) Round and b) triangular localized structure; c) and d) are the corresponding intensity profiles.

smaller for the triangular than for the round structure, though the overall size of the two is comparable if we include the tails.

Each of the two localized structures can be switched on by an appropriate addressing pulse. Lower intensity pulses trigger a round state, higher intensity ones a triangular state. In these regards, the observed weak sensitivity to the addressing intensity suggests the existence of large basins of attraction for each localized structure.

Super-Peaks

In the same nonlinear optical experiment we have recently reported a new type of localized structures, that we call localized peaks, appearing as bright isolated states over a spatial pattern of lower amplitude [35]. These localized peaks correspond to local connections between two different pattern states, each one associated to one of the multistable branches of the system (see Fig. 3). At difference with the previous cases, where a localized state, either round or triangularly shaped, connects an homogeneous state to a modulationally unstable state, localized peaks require bistability between two modulationally unstable states.

In the experiment, we fix a *rms* value of $V_0 = 12.3\,\mathrm{V}$ (frequency 6 KHz) and we vary the input intensity I_{in}. Around this value of V_0, we observe three branches of stationary homogeneous states. The linear stability analysis of these solutions shows that each branch becomes modulationally unstable with respect to a transverse mode, thus generically leading to three patterns that we will call, for simplicity, P_1, P_2 and P_3, respectively.

By increasing I_{in}, we first observe the homogeneous steady state bifurcating to a pattern, P_1, and then localized high amplitude peaks appearing over the pattern. We have named these localized states P_{12}, as they come from the nucleation of a second pattern, P_2, into

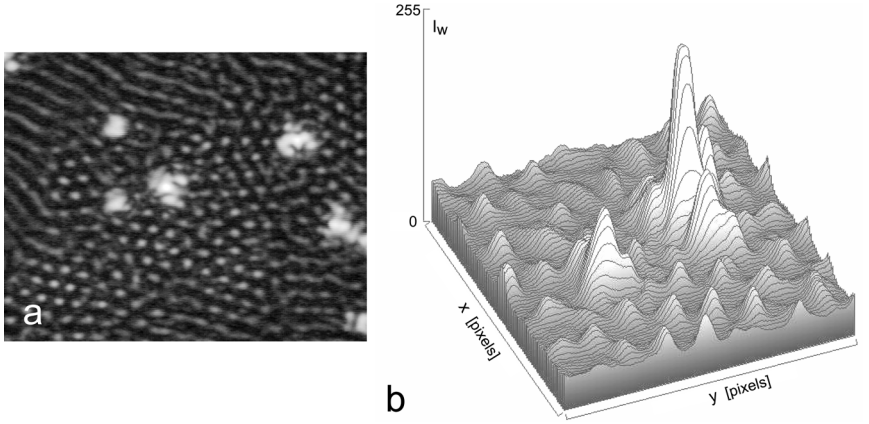

FIGURE 7 a) Instantaneous snapshot showing the simultaneous presence of P_{12} and P_{13} localized peaks; $I_{in} = 0.40\,\mathrm{mW/cm^2}$; b) reconstructed profile of a region containing P_{12} and P_{13}.

the first one, P_1. By further increasing I_{in}, higher amplitude localized peaks appear, P_{13}, that correspond to the nucleation of a third pattern, P_3, into P_1. For intermediate values of I_{in}, as in Figure 7, P_{12} and P_{13} localized peaks coexist in the same spatial regions. By continuing increasing I_{in}, P_{13} peaks dominate over P_{12} and start to invade all the available space, until a densely covered, uniform P_3 pattern is formed. It is worth noting that creation and motion of localized peaks are spontaneously triggered by amplitude and phase fluctuations of the underlying pattern P_1.

We show in Figure 8 the experimental bifurcation diagram: the pattern peak intensity $\langle I_p \rangle$ is plotted as a function of the input intensity I_{in}. The successive branches correspond, respectively, to the homogeneous steady state, then loosing stability with respect to P_1, and then to P_{12}, P_{13} peaks, this last one becoming P_3 for high I_{in}. For each value of I_{in}, $\langle I_p \rangle$ is measured as an average of the pattern maxima by adopting the following procedure. By means of a computer interfaced CCD camera, we record several near-field images. Then, we apply a threshold, in order to keep only the maxima of the patterns, and we make an ensemble average over all the remaining maxima. When two different states, such as P_1 and P_{12}, coexist in the same image we apply a double threshold filtering, in such a way to single out the low and high amplitude state into two separate frames, respectively. Then, the two values of $\langle I_p \rangle$ are measured by making the ensemble average of all the maxima over each frame. This gives, at the same

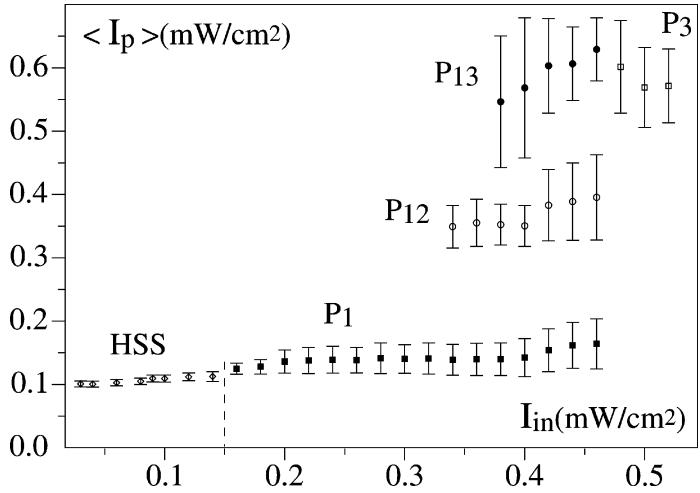

FIGURE 8 Experimental bifurcation diagram, $\langle I_p \rangle$ as a function of I_{in}, for a fixed $V_0 = 12.3\,\mathrm{V}$. The three branches correspond to P_1, P_{12}, and $P_{13} \rightarrow P_3$, respectively. HSS is the homogeneous steady state bifurcating to P_1. The length of the error bars is the standard deviation of $\langle I_p \rangle$.

time, the value of pattern P_1 and that of P_{12} peaks. When P_{12} and P_{13} peaks coexist, to distinguish between them we apply to the near-field images a third threshold filtering, that separates the P_{13} peaks from the rest of the image, and we use the same procedure as before to evaluate the corresponding $\langle I_p \rangle$. When decreasing I_{in}, we observe, both for P_{12} and P_{13}, the same bifurcation diagram as the one for increasing I_{in}. Indeed, hysteresis is prevented by the noise induced mechanism of localized peaks creation, as these events are mainly driven by the amplitude fluctuations of P_1.

Patterns P_1, P_2, and P_3 are not only identified by the different values of their amplitude but also by their different spatial wavelengths, d_i, and corresponding wave numbers, $q_i = 2\pi/d_i$, $i = 1, 2, 3$. We can account for the change of the pattern critical wave number by performing a linear stability analysis of the stationary solutions θ_0 of the LCLV model [25]. The predicted unstable modes provide a fair qualitative agreement with the wave number change accompanying the appearance of localized peaks and the transition from P_1 to P_3 [35].

CONTROL OF THE SPACE-TIME CHAOTIC DYNAMICS

We have recently shown experimental evidence of controlling spatio-temporal chaos by means of a real-space/real-time feedback

technique, which allows stabilization and targeting of two dimensional stationary patterns with arbitrary symmetry and shape. This is realized by applying a perturbing control fields directly in the real space (near-field) in contrast to Fourier space (far-field), used in [36,37] and in times shorter than the characteristic time of the pattern dynamics. As a result, stationary non-homogeneous patterns of arbitrary complexity can be indifferently targeted and stabilized with good efficiency. Our control strategy also offers dynamical flexibility in switching from one to another target pattern, without the need of removing optical components (e.g., filters) in the control loop.

Experimental Scheme

The experimental setup is sketched in Figure 1a. It consists of a main optical feedback loop hosting a LCLV, and of an additional electro-optic control loop. The latter is essentially constituted by a video-camera, a personal computer driving a liquid crystal display (LCD), and a laser beam which traverses the LCD before being injected into the main optical loop. The LCD display, operating in transmission, encodes linearly the gray level output images set on the PC, into an intensity modulations of the laser beam which is traversing it.

When the control loop is open, a homogeneous wave is sent onto the front face of the LCLV, and is reflected acquiring a spatial phase modulation. The beam propagates within the main optical loop from the front face of the LCLV to the input plane of the fiber bundle, experiencing diffraction, and thus converting phase into amplitude modulations. In the present set of experiments, there is no polarization interference ($\psi_1 = \psi_2 = 0^\circ$) and only diffractive feedback is active. Thus, the feedback intensity I_{fb} reaching the rear side of the photoconductor is a nonlinear and nonlocal function of the nonlinear phase shift $\varphi_0 = \beta \cos^2 \theta$ experienced by the light when traversing the liquid crystal layer (θ being the liquid crystal reorientation angle). More precisely,

$$I_{fb}(x,y) = |e^{i\frac{k}{2L}\nabla^2} \perp e^{-i\varphi_0}|^2 I_{in}, \tag{1}$$

where $k = 2\pi/\lambda$ is the optical wave number and $\nabla_\perp$ is the transverse Laplacian.

By increasing of the pump intensity, I_{in}, the homogeneous solution destabilizes, giving rise, close to threshold, to regular hexagonal patterns. When the pump is further increased, hexagons loose stability in favour of space-time chaotic dynamics [31,38]. Together with the pump value, another parameter of the utmost importance is the spatial frequency bandwidth of the system [37], controlled by the

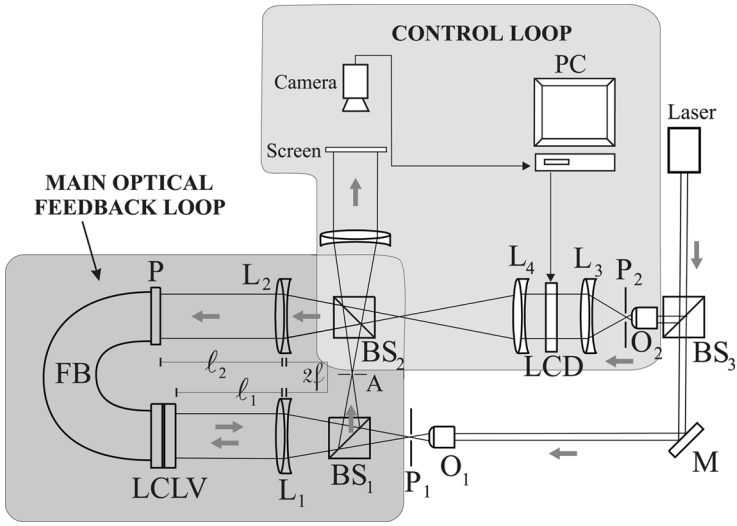

FIGURE 9 Experimental setup. Main loop: an expanded laser beam is closed through a LCLV; M: mirror; O_1: microscope objectives; P_1: pinhole; A: aperture; BS_1, BS_2: beam splitters; L_1, L_2: lenses of focal lens f; L_5: additional lens; FB: fiber bundle. The effective free propagation length is $2f - (l_1 + l_2) = +90$ mm. Control arm: O_2: microscope objectives; P_2: pinhole; BS_3: beam splitters; LCD: liquid crystal display; L_3, L_4: lenses.

aperture A in Figure 9. This aperture is located in a Fourier plane of the main optical loop, and plays a key role in determining the "level of turbulence" of the free-running signal. However, the simple limitation of the Fourier bandwidth is not sufficient to stabilize any pattern.

Pattern Control and Targeting

In order to achieve control over the dynamics, a fraction of the beam traveling in the main optical loop is extracted and recorded by a videocamera, which is interfaced to the PC via a frame grabber. The computer processes the input image, and sends a suitable driving signal to the LCD. The LCD transfer function $T(x, y)$ can be written as the contribution of a constant mean transfer coefficient T_0, plus a modulation signal $s(x, y)$. This modulation s is chosen to be proportional to the error signal between the current pattern intensity I_{fb} present in the system, and a target pattern $I_T(x, y)$:

$$s(x,y,t) = -\beta(I_{fb}(x,y,t) - I_T(x,y)). \tag{2}$$

The digital processing operations performed by the PC include the evaluation of the above error signal, and the calculation of the cross-correlation between pattern and target. The entire time series of pattern is also recorded on the hard disk for further off-line processing.

The resulting refreshing time for the above procedure is at most 200 ms, to be compared to the characteristic time of the pattern dynamics (computed from the decay of the autocorrelation function) which is of the order of the second. The spatial resolution of the feedback signal is also an important parameter for control. The typical length scale of the patterns is $\sqrt{2\lambda L} \simeq 300\,\mu\text{m}$ for $L = 90\,\text{mm}$, the free propagation length set in the main optical loop. The selected area for control is of $1200 \times 1200\,\mu\text{m}$, upon which a control signal of 128×128 pixels is sent. Thus, a typical pattern wavelength is covered by 35–40 pixels. We expect that a substantial decrease of either the spatial or the temporal resolution would limit the efficiency of the control.

The LCD is illuminated with a uniform intensity I_0, and the output beam is imaged onto the rear side of the LCLV. Following the above discussion, this beam will consist of a constant term $T_0 I_0$ that acts in renormalizing the LCLV working point φ_0 to φ_0', plus a modulated controlling beam sI_0. The equation of motion when the control loop is closed is therefore:

$$\frac{\partial \varphi}{\partial t} = -\frac{1}{\tau}(\varphi - \varphi_0') + D\nabla_\perp^2 \varphi + \alpha(I_{fb} - \gamma(I_{fb} - I_T)). \tag{3}$$

where $\gamma \equiv \kappa I_0$.

We initially set the light intensity at the input of the feedback loop to be $I_{in}/I_c \sim 3.2$, where I_c is the critical value for pattern formation from the uniform state to hexagons. In these conditions, the uncontrolled evolution brings the system to display a time evolving, spatially disordered pattern, where many defects are continuously created and annihilated within an hexagonal-like pattern, thus generating STC [38]. A typical snapshot of the uncontrolled dynamics is reported in Figure 1b. Figure 1c reports the space-time dynamical evolution of the central vertical line of pixels in Figure 1b, showing how the uncontrolled dynamics evolves within STC, with a non stationary complex local dynamics and a decaying spatial correlation.

Starting from these conditions, three different target patterns are selected, namely perfect hexagons, squares and a particular snapshot of the uncontrolled dynamical evolution (shown in the top row of Fig. 10). Regular hexagons are a stable solution close to the pattern formation threshold, thus the use of hexagons as a target tests the ability of the method to control a solution normally unstable when the distance from threshold increases. On the other hand, using as

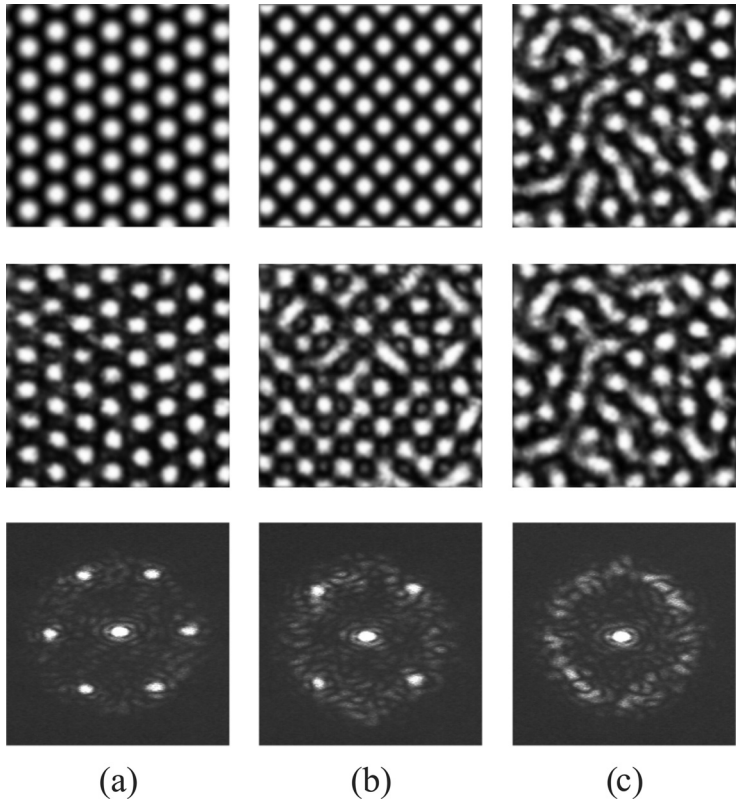

FIGURE 10 Examples of target patterns (top row), controlled area in the system at $\gamma = 0.4$ (center row) and corresponding far field images (bottom row) for the control trials of a perfect hexagonal pattern (a), a square pattern (b), and a snapshot of the uncontrolled dynamics (c).

target a snapshot of the uncontrolled dynamics assesses the robustness of the method to freeze a given natural state of the uncontrolled dynamics, in the same spirit as the so called targeting of chaos [39]. Finally, squares are never spontaneously selected by the system without control, and thus they serve us to assess the ability of the control strategy to force the appearance of any arbitrary symmetry. The results obtained for $\gamma = 0.4$ in the three cases are reported in the center row of Figure 10, indicating that the control procedure is successful in all cases.

The bottom row of Figure 10 shows the far field images of the controlled dynamics. While hexagonal and square patterns have a rather simple global symmetry, thus allowing for an easy implementation of Fourier filtering techniques, like the one of Ref. [36], the target STC

snapshot involves the presence of a complicate power spectrum. The fabrication of Fourier masks reproducing the amplitude and phase of these patterns appears extremely difficult in experiments.

To demonstrate the high flexibility of our control technique, we have prepared a time-dependent target pattern formed by the following ordered sequence: a snapshot of the uncontrolled dynamics, a square pattern and a hexagonal pattern. Each snapshot is presented to the system for a time $T = 20$ s, and intermingled with periods of $T = 20$ s, during which the system is left uncontrolled. The control ability of the method is evaluated by calculating the time dependent correlation function $C(t) = \langle I_{fb}(\mathbf{r}, t) \cdot I_T(\mathbf{r}) \rangle$ **r** between the instantaneous pattern and the target one ($\langle \ldots \rangle$ **r** denotes a spatial average). The results are shown in Figure 11, where C(t) is plotted as a function of time. It can be seen that the system is able to attain each one of the sequenced target pattern for the same value of $\gamma = 0.4$, as well as to switch between the different patterns. Notice that each target pattern in the sequence produces a different state in the correlation,

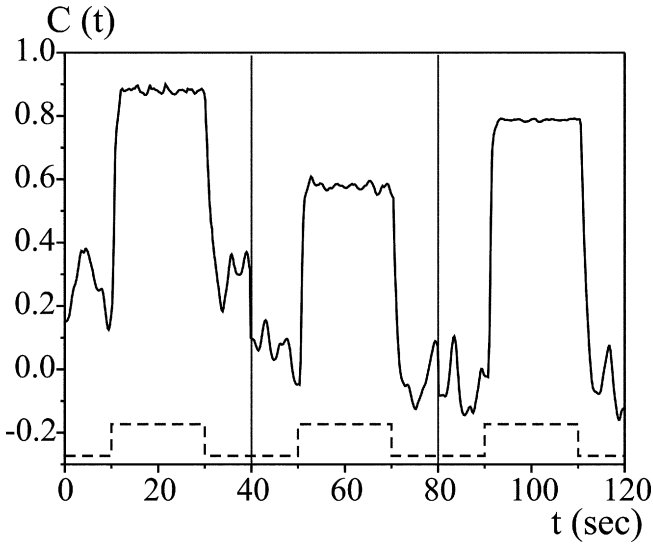

FIGURE 11 Correlation function $C(t)$ *vs*. time during the sequential control trial at $\gamma = 0.4$. The target patterns are a snapshot of the uncontrolled dynamics ($10 \leq t < 30$ sec), a square pattern ($50 \leq t < 70$ sec) and a hexagonal pattern ($90 \leq t < 110$ sec). The dashed line indicates the switching on/off times. The vertical lines separates the three domains in time in which a different pattern is taken as target for the control. In each time domain, the correlation is calculated using the corresponding target pattern.

depending upon its specific instability features within the uncontrolled regime. The maximal correlation is obtained for the snapshot of the uncontrolled dynamics, since this pattern represents a specific state compatible with the uncontrolled dynamics.

Space-Time Chaos Synchronization

In recent years, synchronization of complex systems have attracted a great interest in the scientific community [40]. Recently, we have shown that a complete synchronization on unidirectionally coupled patterns can be achieved in a LCLV with optical feedback [28]. The experimental setup is the same as the one sketched in Figure 9, comprising a LCLV within the main optical feedback loop and a LCD inside a coupled control loop.

With the help of such a real-space/real-time control technique we aim now to demonstrate complete synchronization in a unidirectionally coupled scheme between two identical systems in a regime of spatio-temporal chaos. At this purpose, we initially let the control loop open and record over a time interval T the free evolution of the system for a value of I_{in} at which the uncontrolled dynamics displays space-time chaos. We refer to this sequence of images as the Master Dynamics (MD). After the registration of the MD, further free evolution is granted to the uncontrolled system, so that after a few seconds the output of the main optical loop is totally uncorrelated with the initial frame of the MD. At this point, we close the control loop and we replay the registered MD as the target pattern $I_T(x,y,t)$. In this way, we are implementing a unidirectional coupling scheme between two *identical* systems starting from fully uncorrelated initial conditions. By repeating the replaying procedure of the MD with increasing values of γ, the coupling strength, we eventually observe full synchronization between the controlled output of the main optical loop, the Slave Dynamics (SD), and the MD.

Complete synchronization between SD and MD is obtained for $\gamma = 0.8$. A way for visualizing the emergence of a complete synchronization is to pick randomly a set of N points $[(x_i,y_i); i = 1,\ldots,N]$ in both the MD and the SD, and to plot the variable $x_{SD}(t) = \{I_{fb}\ (x_i,y_i,t),\ i=1,\ldots,N\}$ *vs.* the corresponding variable $x_{MD}(t) = \{I_T\ (x_i,y_i,t), i=1,\ldots,N\}$. The more the distribution of points in the (x_{SD},x_{MD}) plane approaches the synchronization manifold (the diagonal line $x_{SD}=x_{MD}$), the more complete is the synchronization that sets in the system at all times. Experimental results are reported in Figure 12 for two values of the coupling strength γ. Precisely, Figure 12a and 12c shows the distribution of points in the (x_{SD},x_{MD})

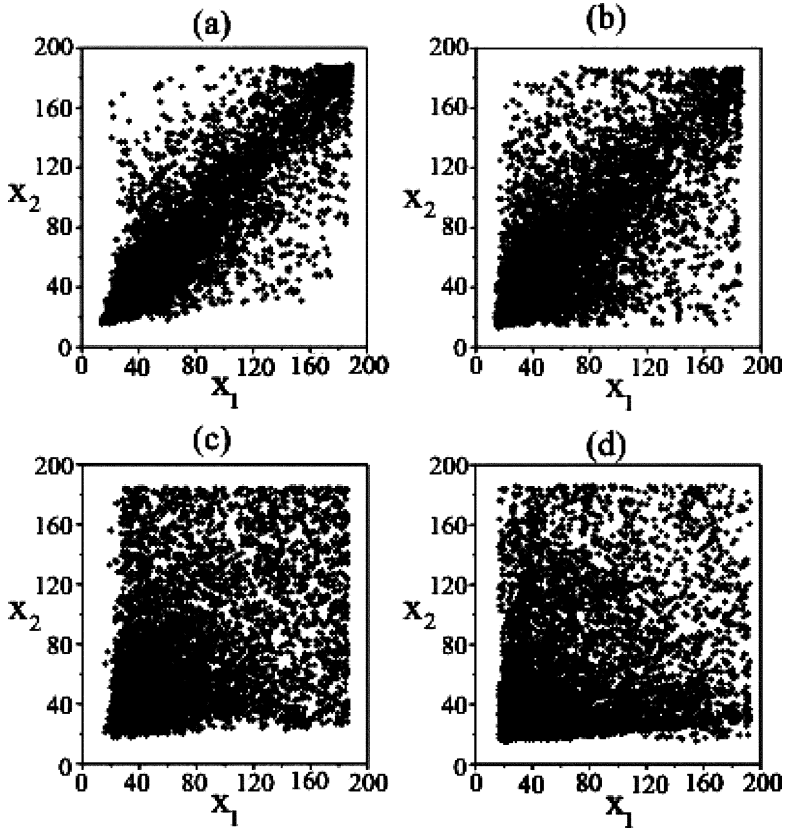

FIGURE 12 Experimental point distributions in the (x_{SD}, x_{MD}) plane. The synchronization manifold is represented by the diagonal line $(x_{SD}=x_{MD})$. (a) $I=2$, $\gamma=0.8$, (b) $I=3$, $\gamma=0.8$, (c) $I=2$, $\gamma=0$, (d) $I=3$, $\gamma=0$.

plane for $I=2$ and $\gamma=0.8$ ($\gamma = 0$), while Figure 12b and 12d refers to the same situation for $I=3$ and $\gamma = 0.8$ ($\gamma=0$). In both cases, it is evident that increasing the coupling strength induces a point distribution much closer to the diagonal line than the uncoupled case, thus proving that the two coupled systems approach a complete synchronization.

CONCLUSIONS

In a nonlinear optical interferometer, formed by a LCLV with feedback, we have reviewed a set of experiments dealing with the appearance of spatial structures and the control of their spatio-temporal

dynamics. We have shown that for certain regimes of parameters the response of the LCLV is similar to that of a binary phase slice, working around a point of bistability. In these conditions, we observe stable localized structures. Depending on the type of the bistable branches, corresponding either to spatially homogeneous states or to modulationally unstable states, different kinds of localized structures can appear, differing both in their shape and in their peak amplitude. The richness of the observed localized states is enlarged by the complexity of their dynamics, displaying bouncing and interaction between adjacent structures. The manipulation and control of such dynamical state can be exploited for applications in the field of optical information storage and processing [33].

In the case when the optical feedback is purely diffractive and the LCLV system displays spatially extended structures, we have demonstrated a control technique, allowing the targeting of a selected pattern among a complex state of the space-time chaos characterizing the full dynamics. Our control method operates in the real space (near-field) and, at variance with the methods operating in the Fourier space (far-field), offers a great flexibility in the dynamical switching between different target patterns. Finally, by applying a similar technique, we have demonstrated that two identical pattern forming systems can be coupled in such a way that a complete synchronization of the slave to the master dynamics is induced. Once again, the great flexibility offered by the proposed coupling scheme can be exploited to drive the slave system onto a generic desired dynamics with arbitrary symmetry and shape in space, as well as arbitrary behaviors in time.

As further developments, control techniques have to be applied when the LCLV displays localized structures. In such a case, each single localized state acts as an elementary pixel of information. Their control and synchronization will open the way to the successful implementation of optical devices dedicated to the storage and parallel processing of spatially distributed information.

REFERENCES

[1] Nicolis, G. & Prigogine, I. (1977). *Self-Organization in Non Equilibrium Systems*, J. Wiley & Sons: New York.
[2] Cross, M. & Hohenberg, P. (1993). *Rev. Modern Phys.*, *65*, 581.
[3] Fauve, S. & Thoual, O. (1990). *Phys. Rev. Lett.*, *64*, 282.
[4] Eschenfelder, H. A. (1981). *Magnetic Bubble Technology*, Springer Verlag: Berlin.
[5] Pirkl, S., Ribiere, P., & Oswald, P. (1993). *Liq. Cryst.*, *13*, 413.
[6] Astrov, Y. A. & Logvin, Y. A. (1997). *Phys. Rev. Lett.*, *79*, 2983.

[7] Lee, K.-J., McCormick, W. D., Pearson, J. E., & Swinney, H. L. (1994). *Nature*, *369*, 215.
[8] Edwards, W. S. & Fauve, S. (1994). *J. Fluid Mech.*, *278*, 123.
[9] Umbanhowar, P. B., Melo, F., & Swinney, H. L. (1996). *Nature*, *382*, 793.
[10] Heinrichs, R., Ahlers, G., & Cannell, D. S. (1987). *Phys. Rev. A*, *35*, R2761.
[11] Kolodner, P., Bensimon, D., & Surko, C. M. (1988). *Phys. Rev. Lett.*, *60*, 1723.
[12] Mc Laughlin, D. W., Moloney, J. V., & Newell, A. C. (1983). *Phys. Rev. Lett.*, *51*, 75.
[13] McDonald, G. S. & Firth, W. J. (1993). *J. Opt. Soc. Am. B*, *10*, 1081.
[14] Tlidi, M., Mandel, P., & Lefever, R. (1994). *Phys. Rev. Lett.*, *73*, 640.
[15] Brambilla, M., Lugiato, L. A., & Stefani, M. (1996). *Europhys. Lett.*, *34*, 109.
[16] Firth, W. & Scroggie, A. J. (1996). *Phys. Rev. Lett.*, *76*, 1623.
[17] Saffman, M., Montgomery, D., & Anderson, D. Z. (1994). *Opt. Lett.*, *19*, 518.
[18] Taranenko, V. B., Staliunas, K., & Weiss, C. O. (1997). *Phys. Rev. A*, *56*, 1582.
[19] Neubecker, R., Oppo, G. L., Thuering, B., & Tschudi, T. (1995). *Phys. Rev. A*, *52*, 791.
[20] Ramazza, P. L., Ducci, S., Boccaletti, S., & Arecchi, F. T. (2000). *J. Opt. B*, *2*, 399.
[21] Schaepers, B., Feldmann, M., Ackemann, T., & Lange, W. (2000). *Phys. Rev. Lett.*, *85*, 748.
[22] Taranenko, V. B., Ganne, I., Kuszelewicz, R. J., & Weiss, C. O. (2000). *Phys. Rev. A*, *61*, 063818.
[23] Coullet, P. (2002). *International Journal of Bifurcation and Chaos*, *12*, 2445 and references therein.
[24] Clerc, M. G., Petrossian, A., & Residori, S. (2005). *Phys. Rev. E*, *71*, 015205.
[25] Clerc, M. G., Residori, S., & Riera, C. S. (2001). *Phys. Rev. E*, *63*, 060701 (R); Clerc, M. G., Nagaya, T., Petrossian, A., Residori, S., & Riera, C. S. (2004). *Eur. Phys. J. D*, *28*, 435.
[26] Bortolozzo, U., Pastur, L., Ramazza, P. L., Tlidi, M., & Kozyreff, G. (2004). *Phys. Rev. Lett.*, *93*, 253901.
[27] Pastur, L., Gostiaux, L., Bortolozzo, U., Boccaletti, S., & Ramazza, P. L. (2004). *Phys. Rev. Lett.*, *93*, 063902.
[28] Ramazza, P. L., Bortolozzo, U., & Boccaletti, S. (2006). *Phys. Rev. E* (in press).
[29] Akhmanov, S. A., Vorontsov, M. A., & Ivanov, V. Yu. (1988). *JETP Lett.*, *47*, 707.; Vorontsov, M. A. & Miller, W. B. (1995). In: *Self-Organization in Optical Systems and Applications in Information Technology*, Vorontsov, W. B. & Miller, W. B. (Eds.), Springer: Berlin.
[30] Arecchi, F. T., Boccaletti, S., Ducci, S., Pampaloni, E., Ramazza, P. L., & Residori, S. (2000). *J. of Nonlinear Opt. Phys. & Materials*, *9*, 183.
[31] D'Alessandro, G. & Firth, W. J. (1992). *Phys. Rev. A*, *46*, 537.
[32] Ramazza, P. L., Benkler, E., Bortolozzo, U., Boccaletti, S., Ducci, S., & Arecchi, F. T. (2002). *Phys. Rev. E*, *65*, 066204–1.
[33] Hayasaki, H., Yamamoto, H., & Nishida, N. (2003). *Opt. Lett.*, *28*, 2351.
[34] Pomeau, Y. (1986). *Physica D*, *23*, 3.
[35] Bortolozzo, U., Rojas, R., & Residori, S. (2005). *Phys. Rev. E*, *72*, 045201.
[36] Jensen, S. J., Schwab, M., & Denz, C. (1998). *Phys. Rev. Lett.*, *81*, 1614; Ackemann, T., Giese, B., Schäpers, B., & Lange, W. (1999). *J. Opt.*, *B1*, 70; Harkness, G. K., Oppo, G. L., Benkler, E., Kreuzer, M., Neubecker, R., & Tschudi, T. (1999). *J. Opt.*, *B1*, 177; Benkler, E., Kreuzer, M., Neubecker, R., & Tschudi, T. (2000). *Phys. Rev. Lett.*, *84*, 879.
[37] Mamaev, A. V. & Saffman, M. (1998). *Phys. Rev. Lett.*, *80*, 3499.
[38] Neubecker, R., Thuring, B., Kreuzer, M., & Tschudi, T. (1999). *Chaos, Solitons and Fractals*, *10*, 681.

[39] Boccaletti, S., Grebogi, C., Lai, Y. C., Mancini, H., & Maza, D. (2000). *Phys. Rep.*, *329*, 103, and references therein.
[40] Boccaletti, S., Kurths, J., Osipov, G., Valladares, D., & Zhou, C. (2002). *Phys. Rep.*, *366*, 1, and references therein.